Rate Constants for the Hydrogen Abstractions in the OH-Initiated Oxidation of Glycolaldehyde. A Variational Transition-state Theory Calculation

Montserrat Ochando-Pardo,[†] Ignacio Nebot-Gil,[†] Angels González-Lafont,*[,‡] and José M. Lluch[‡]

Departament de Química Física and Institut de Ciència Molecular, Universitat de València, 46100 Burjassot, Spain, and Departament de Química, Universitat Autònoma de Barcelona, 08193 Bellaterra, Barcelona, Spain

Received: December 31, 2003; In Final Form: March 1, 2004

The reaction between the OH radical and glycolaldehyde has been theoretically studied for the first time. By means of preliminary MP2(FC)/6-31G*, B3LYP/6-31G*, CBS-Q, G2, and G3 electronic structure calculations, two main processes have been determined, $CH_2OHCHO + OH \rightarrow CH_2OHCO + H_2O$ and $CH_2OHCHO + OH \rightarrow CHOHCHO + H_2O$, in clear agreement with experimental data. Then the variational transition-state theory rate constants with multidimensional tunneling corrections (when necessary) (VTST-MT) have been calculated using dual-level interpolation algorithms. The theoretical rate constant for the global process at 298 K of 3.83×10^{-11} cm^3 molecule^{-1} s^{-1} is in reasonable agreement with the experimental value. In the temperature range 100−350 K, we predict a clear inverse dependence of the global rate constant on temperature.

1. Introduction

The oxidation of organic compounds as alkanes and alkenes provides hydroxycarbonyls among other products in the low atmosphere.[1] The simplest hydroxycarbonyl is glycolaldehyde, CH_2OHCHO, and its presence in the atmosphere is mainly due to the oxidation of ethene and isoprene, as well as the direct emission in biomass fires.[2,3] Although the atmospheric fate of glycolaldehyde is at present not well defined, it is known that the most important processes in which glycolaldehyde participates in the troposphere during daytime are its oxidation by the OH radical and its photolysis. Both processes have been studied very little experimentally,[2,3] and to our knowledge, no theoretical calculation on this matter has been published.

For the oxidation of glycolaldehyde by the OH radical, four reactions are possible

$$CH_2OHCHO + OH \rightarrow CH_2OHCO + H_2O \quad (R1)$$

$$CH_2OHCHO + OH \rightarrow CHOHCHO + H_2O \quad (R2)$$

$$CH_2OHCHO + OH \rightarrow CH_2OCHO + H_2O \quad (R3)$$

$$CH_2OHCHO + OH \rightarrow CH_2OHC(OH)HO \quad (R4)$$

In the two available experimental studies of these reactions,[2,3] the rate constant for the consumption of the OH radical was measured at 298 K and at nearly 1 atm of pressure. Data are only available at a single temperature, so that activation energy could not be determined in either of those two experimental studies. However, in both cases, an analysis of the products was made to determine the major process among the possible reactions that can occur. According to Niki et al.,[2] approximately 80% of the yield of the process is due to the abstraction of the hydrogen atom bonded to the carbonyl group (reaction R1), whereas the other 20% corresponds to the abstraction of the hydrogen atom bonded to the other carbon atom (reaction R2). The influence of the other two reactions (R3 and R4) in the global process is negligible. To study the OH-initiated oxidation of glycolaldehyde, Niki et al. employed the FTIR spectroscopic method. They obtained a rate constant value for this process of $(1.0 \pm 0.2) \times 10^{-11}$ cm^3 molecule^{-1} s^{-1} determined by measuring its relative rate with reference to the rate of acetaldehyde OH-initiated oxidation. Later, Bacher et al.[3] used the FTIR absorption spectrometry technique in an environmental chamber to study the same reaction. They obtained a rate constant value of $(1.1 \pm 0.3) \times 10^{-11}$ cm^3 molecule^{-1} s^{-1} for the overall OH-initiated oxidation of glycolaldehyde measured as a weighted average of the relative rates of this process to two reference reactions, namely, the OH-initiated oxidation of propene and the OH-initiated oxidation of acetaldehyde. The agreement between the experimental rate constants of Niki et al.[2] and Bacher et al.[3] is remarkable.

In the current work, the first theoretical study of the oxidation reaction of glycolaldehyde by the OH radical is carried out. To this aim, we have calculated the hydrogen abstraction rate constants corresponding to reactions R1 and R2, and the rate constant corresponding to the global process, as a function of temperature by employing high level electronic structure calculations and the variational transition-state theory with multidimensional tunneling corrections (when necessary)[4,5] (VTST-MT). This oxidation reaction constitutes an example of a very fast gas-phase oxidation process. Our purpose is to use theory to understand the detailed mechanism and kinetics of this reaction and to obtain useful information that has not been attained experimentally yet. In section 2, the details of the electronic structure calculations and the dynamic methodology are given. In section 3, the theoretical results are commented, and in section 4, the conclusions of the present work are presented.

* To whom correspondence should be addressed. E-mail: angels@klingon.uab.es.
[†] Universitat de València.
[‡] Universitat Autònoma de Barcelona.

10.1021/jp031363z CCC: $27.50
Published on Web 05/18/2004

2. Methodology

In this section, we will give the details of the electronic structure calculations and the dynamic methodology used in this study.

2.A. Electronic Structure Calculations. The geometries of all of the species implicated in the different reactions between OH and glycolaldehyde, from R1 to R4, have been optimized, and the nature of the stationary points, saddle points or minima, was determined by means of the analysis of the number of imaginary frequencies (NIMAG = 1 or 0, respectively). A preliminary study was carried out to determine which are the most suitable electronic methods for describing the reactions under study. We used ab initio methods, hybrid density functional theory (DFT), and multilevel techniques trying to predict kinetic data as accurately as possible. The methods chosen were HF, MP2(FC), and B3LYP with the 6-31G* basis set, as well as the CBS-Q,[6] G2,[7] and G3[8] schemes.

To further improve the description of the potential energy surface, two recent modifications of the G3 technique were also used: the scaled G3 technique (G3S),[9] and the minimal multicoefficient G3 technique (MMCG3).[10] The G3S technique is a modification of G3 method, in which scale factors are used to multiply each term that contributes to the total energy instead of the additive higher level correction (HLC) of the original formulation. The MMCG3 technique also uses multiplicative factors instead of additives terms, but modifications in the way higher-order correlation energies are divided and in the basis set extension of the multilevel energy expression make this method less time-consuming. On the other hand, the G3S parameters were optimized with a larger test set of energies than the one used for the MMCG3 coefficients. The main advantage of these two more recent G3 formulations is that they can be used to calculate potential energy surfaces because the energy expression is a continuous function of the geometry due to the elimination of the higher level correction term of previous Gn methodologies. This aspect makes those techniques more interesting from a dynamic point of view.

The first step of the G3S methodology is the geometry optimization at the MP2(full)/6-31G* level. These MP2(full)/6-31G* geometries are then used for subsequent single-point energy calculations. For comparison purposes in the preliminary study, the MMCG3 classical energies have been evaluated at those same MP2(full)/6-31G* geometries.

After the preliminary study, the geometries of the stationary points of reactions R1 and R2 have been optimized and characterized by the analysis of first and second derivatives at the MP2(full)/6-31G* level. The classical energy at those stationary points has been obtained at this electronic level and also using the G3S methodology. Note that, in our particular application of the G3S methodology for the dynamic calculations presented in this paper, we use scaled MP2(full)/6-31G* zero-point energies (ZPEs) (scaling factor of 0.9661[11]) instead of scaled HF/6-31G* ZPEs as in the original G3S formulation. Moreover, in Gn and modified Gn procedures, the geometry choice is considered part of the method. However, in other multilevel approaches, even if a geometry was chosen for obtaining parameters and calculating mean errors, the use of the same multilevel energy expression with different geometries has been considered perfectly acceptable. Following this last strategy, in this study, we have also proved another modification of the G3S technique in which the geometry optimization is performed at the QCISD/6-31G* level. The aim of this modification is to improve MP2 geometries and frequencies because it has been shown that the presence of even a small amount of spin contamination in UHF wave functions can cause significant errors in calculated vibrational frequencies at the UMP2 level.[12] For this reason, the stationary points of reactions R1 and R2 have also been optimized and characterized at the QCISD/6-31G* level, whose frequencies have been scaled using a factor of 0.9776.[11] The classical potential energy at those stationary points has been obtained at the QCISD/6-31G* level and also using the G3S methodology.

As it will be detailed in the Results and Discussion section, both reactions R1 and R2 were found to occur following the same general scheme (see Figure 1): first, there is the formation of a complex in the entrance channel which then can lead to the corresponding hydrogen abstraction pathway. The two associations of reactants in R1 and R2 take place without saddle point, whereas each abstraction process has one. The two abstraction pathways also present a complex in their respective product sides which dissociates leading to the final products in each case.

For the association regions, that is, the formation of the complexes CR1 and CR2 (Figure 1) as the reactants approach each other, we have constructed two distinguished reaction coordinate paths (DCPs) by fixing for each channel the hydrogen-bond distance R(H−O) (depicted in Figure 1) between the oxygen atom of the glycolaldehyde and the hydrogen atom of the OH radical and allowing the other degrees of freedom to relax at the MP2(full)/6-31G* level. A total of 25 nonstationary structures from R(H−O) = 2.101 Å to 4.001 Å and a total of 33 nonstationary structures from R(H−O) = 2.003 Å to 4.653 Å were calculated for R1 and R2, respectively. First and second energy derivatives at the MP2(full)/6-31G* level together with the G3S classical energies were computed at all of those DCP geometries. The generalized normal-mode analysis was performed in Cartesian coordinates within the harmonic approximation and with a scaling factor of 0.9661[11] for the vibrational frequencies. For the dissociation of the product complexes formed after each hydrogen abstraction, no DCPs were calculated as it will be explained below.

The minimum energy paths (MEPs) at the MP2(full)/6-31G* level using the Gonzalez−Schlegel mass-weighted internal coordinates reaction path algorithm[13] for the hydrogen abstraction pathways of reactions R1 and R2 have been calculated. A gradient step size, δs (where s indicates the distance along the MEP), of 0.00529 Å in an isoinertial mass-weighted internal coordinate system[14,15] with a scaling mass equal to 1 amu has been used to follow the MEP. For reaction R1, the MEP has been calculated from $s = -2.0$ bohr to $s = 2.43$ bohr, with $s = 0$ being the saddle point location, positive s values corresponding to the products side and negative s values corresponding to the reactants side. For reaction R2, the MEP extends from $s = -2.84$ bohr to $s = 2.99$ bohr. For the calculation along the MEP of the adiabatic energy profile (classical potential energy plus vibrational ZPE) that is used in VTST, 98 and 55 Hessian matrices of the corresponding nonstationary points were calculated for reactions R1 and R2, respectively. Then, the generalized normal-mode analysis was performed in redundant internal coordinates within the harmonic approximation and with a scaling factor of 0.9661[11] for the vibrational frequencies.

Single-point classical potential energy calculations at some selected geometries along the MP2(full)/6-31G* MEPs were done at the G3S level.

Thermodynamic and quasi-thermodynamic magnitudes have been computed by using the statistical thermodynamic formula-

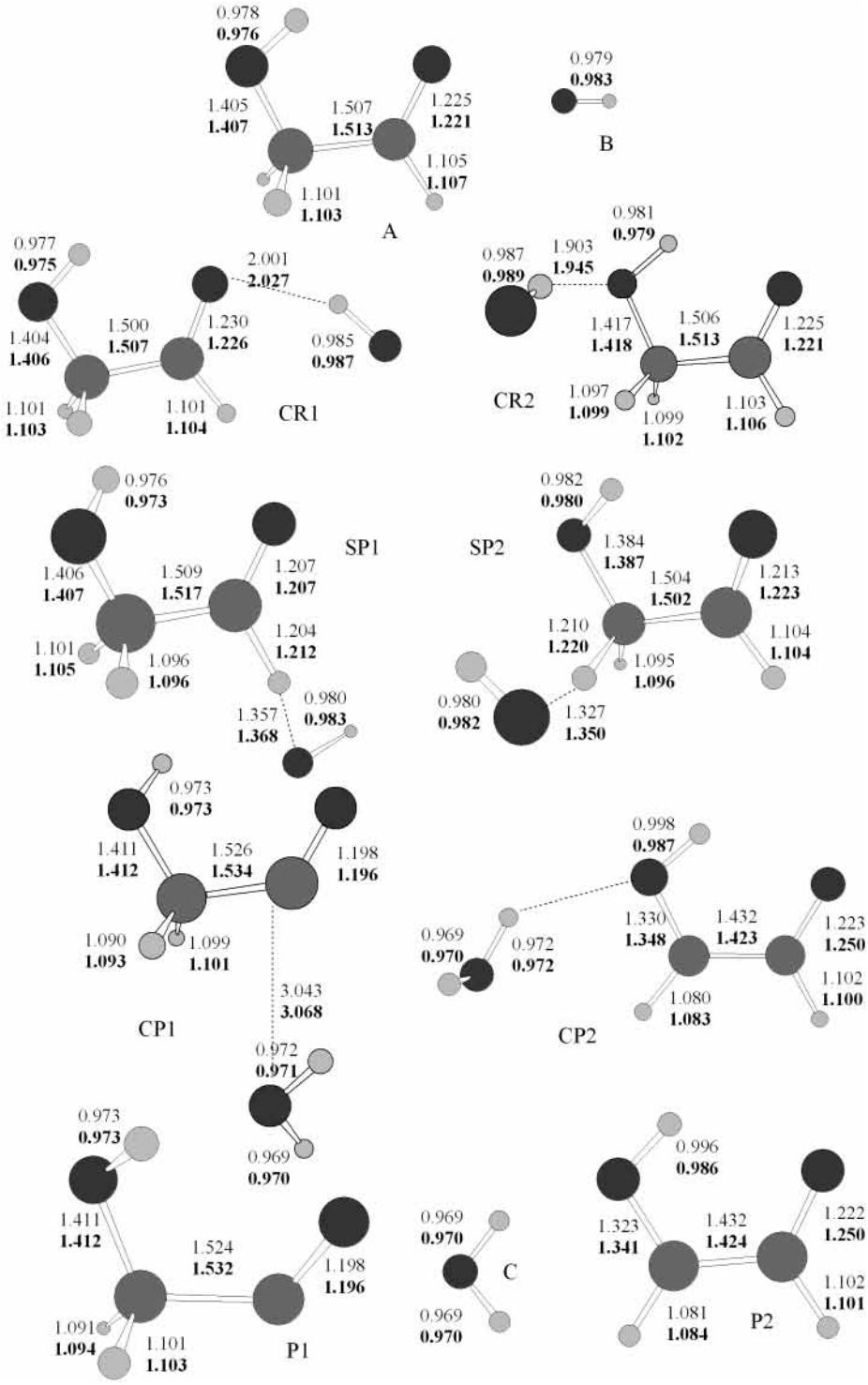

Figure 1. Main geometrical parameters of the stationary points of reactions R1 and R2. A and B are glycolaldehyde and OH, respectively; CR1 and CR2 are the entrance complexes of reaction 1 and 2, respectively; SP1 and SP2 are the saddle point structures of the two reactions; CP1 and CP2 are the corresponding exit complexes; P1 and P2 are the radical products formed in reactions R1 and R2, whereas C is the water molecule formed in both reactions. Normal and bold face numbers correspond to the MP2(full)/6-31G* and QCISD/6-31G* geometries, respectively. Distances are given in Å.

tion of partition functions within the ideal gas, rigid rotor, and harmonic oscillator models.

All of the electronic calculations have been performed using the program system Gaussian 98 in its releases A.6 and A.7.[16]

2.B. Dynamic Calculations. As we have already commented, the reaction of glycolaldehyde with the hydroxyl radical can proceed via two main channels. There are therefore two competitive reactions. To obtain the global reaction rate constant we have applied the competitive canonical unified statistical (CCUS)[17] theory in which the global reaction rate constant, $k^{CCUS}(T)$, is given by

$$k^{CCUS}(T) = k_1(T) + k_2(T) \quad (1)$$

where $k_1(T)$ and $k_2(T)$ are the rate constants for reactions R1 and R2, respectively. For the calculation of these two rate constants, the canonical unified statistical (CUS)[18] theory must be applied because there are several consecutive dynamic bottlenecks along each one of these channels. The CUS

expression for $k_i(T)(i = 1,2)$ is then given by

$$\frac{1}{k_i(T)} = \frac{1}{k_{ASi}(T)} - \frac{1}{k_{CRi}(T)} + \frac{1}{k_{Hi}(T)} \qquad (2)$$

where $k_{ASi}(T)$, and $k_{Hi}(T)(i = 1,2)$ are the one-way flux rate constants for the association regions and the hydrogen abstraction regions, respectively, in R1 and R2. The rate constants $k_{CRi}(T)(i = 1,2)$, are the one-way flux evaluated at each free energy minimum along the reaction path related to the complex formation in the entrance channel. In agreement with the original presentation of CUS theory, the reactant partition function for all of these one-way flux rate constants is the same and corresponds to the asymptotic reactants partition function. Note that the dissociations of the product complexes are not taken into account in the evaluation of $k_{CRi}(T)(i = 1,2)$, as they are not expected to have any effect due to the high exothermicity of the reactions. Despite this, the product complexes are included in the calculation of $k_{Hi}(T)(i = 1,2)$, since their existence modifies the shape of the abstraction-energy profiles. All calculations are for the low-pressure limit of the reaction where bimolecular collisions are not interrupted by collisions with third bodies.

The branching ratios corresponding to R1 and R2 hydrogen abstraction reactions have been defined as

$$\frac{k_i(T)}{k_1(T) + k_2(T)} \times 100 \qquad i = 1, 2 \qquad (3)$$

All of the one-way flux rate constants have been calculated by using the canonical variational transition-state (CVT)[14,15,19−22] theory including multidimensional tunneling contributions (MT) when necessary by means of the small-curvature tunneling (SCT)[23,24] semiclassical adiabatic ground-state approximation. The expression for the CVT/SCT rate constant, used in the temperature range from 100 to 350 K, is the following:

$$k^{CVT/SCT}(T) = \kappa^{SCT}(T) \frac{\sigma k_B T}{h} \frac{Q^{GT}(T,s_*)}{Q^R(T)} \exp(-V_{RP}(s_*)/k_B T) \qquad (4)$$

where $\kappa^{SCT}(T)$ is the SCT transmission coefficient, s_* denotes the value of s at the free energy maximum along the reaction path (DCP in the association regions and MEP in the hydrogen-abstraction regions) at temperature T, σ is the symmetry factor,[25] k_B is the Boltzmann's constant, h is Planck's constant, $V_{RP}(s_*)$ is the classical potential energy at s^* with zero of energy at the overall classical energy of reactants, $Q^R(T)$ is the reactants partition function per unit volume again with zero of energy at reactants, and $Q^{GT}(T,s_*)$ is the partition function of the generalized transition state at s_* with zero of energy at $V_{RP}(s_*)$ and excluding the reaction coordinate. For all of the partition functions, the rotational symmetry numbers are removed, as they are included in σ. These symmetry numbers for each region are calculated according to the expression[26]

$$\sigma(s) = n\sigma^R/\sigma^{GT}(s) \qquad (5)$$

where n stands for the number of kinetically equivalent transition states, σ^R is the usual rotational symmetry number for the reactants (or the product of these symmetry numbers if there are two molecular reactants as in the present case), and $\sigma^{GT}(s)$ corresponds to the usual rotational symmetry number of the generalized transition state at s. In our applications, σ^{GT} is independent of s, and thus, σ(s) becomes a constant σ. In all of the cases studied in this paper $\sigma^R = 1$ and $\sigma^{GT} = 1$. However, $n = 1$ for the association and the hydrogen-abstraction regions of R1, but $n = 2$ for the corresponding regions of R2. This leads to a symmetry number of 1 or 2 for the two regions of R1 or R2, respectively. For the electronic partition function of the OH radical, the excited state $^2\Pi_{1/2}$ (140 cm^{-1}) has also been taken into account.

In this study, initially two different approaches of dual level direct dynamic calculations have been employed. First, for the regions with a saddle point (the two hydrogen-abstractions), an interpolated single-point energy calculation (ISPE)[27] was performed, in which the MEP calculated at the low level (LL) (MP2(full)/6-31G*) was corrected by means of single-point high level (HL) G3S classical potential energies evaluated at the stationary points and at a series of nonstationary points along the MEP. For reaction R1, the LL classical potential energy was corrected at 22 nonstationary points, with these points between $s = -0.80$ and 0.64 bohr. For reaction R2, 21 nonstationary points were used from $s = -1.20$ to 0.52 bohr. In the ISPE approach, the HL classical potential energies and the LL geometries and frequencies are interpolated using a mapping procedure.[28] For the regions without a saddle point (associations), the LL DCPs have also been corrected with G3S HL classical potential energies evaluated at all of the geometries along the reaction path. However, the fit of the information along the DCPs was done by a Lagrangian interpolation of order 3. Note that in this first dual level approach only the classical potential energy is corrected.

The generalized normal-mode analysis at the nonstationary points along the MEPs were carried out[4] by diagonalizing the corresponding projected force constant matrices orthogonal to the gradient and the six directions corresponding to infinitesimal translations and rotations. However, the RODS[29,30] algorithm was applied along the DCPs.

The second dual level direct dynamics approach (only applicable to regions with saddle point structure) used here is called interpolated optimized corrections (IOC)[31−36] method. In the IOC procedure, the LL classical energies, moments of inertia, and frequencies (along the MP2(full)/6-31G* MEPs) are corrected by HL calculations performed only at the stationary points. Those HL calculations have consisted of G3S classical potential energies at the QCISD/6-31G* stationary point geometries including scaled QCISD/6-31G* frequencies. Following the original IOC formulation,[31−33] we should have carried out the optimization and the calculation of second derivatives with the full G3S multilevel energy expression instead of using the geometries and frequencies at the QCISD/6-31G* level. For this reason, we will refer to our particular applications of the IOC scheme as intermediate IOCs.

All dynamic calculations have been carried out using the POLYRATE 8.7. program.[37]

3. Results and Discussion

In section A, the results corresponding to the electronic structure calculations are detailed. Then, in section B, dynamic results are explained.

3.A. Electronic Structure Results. For reactions R1−R4 in Table 1, the classical potential energies of reaction along with the reaction free energies (at $T = 298$ K), the classical potential energy barriers in the hydrogen-abstraction regions, and the free energy barriers (at $T = 298$ K) calculated at the hydrogen-abstraction saddle point structures are given. Note that the standard state for the reaction free energies and the free energy barriers is the ideal gas state when the pressure is 1 atm or the

TABLE 1: Classical Potential Energy of Reaction (ΔV), Free Energy of Reaction (ΔG^0), Classical Potential Energy Barrier Height ($V^{\ddagger}$), and Activation Free Energy ($\Delta G^{\ddagger 0}$) in kcal/mol at 298 K

	R1				R2				R3				R4			
method	ΔV	ΔG^0	$V^{\ddagger}$	$\Delta G^{\ddagger 0}$	ΔV	ΔG^0	$V^{\ddagger}$	$\Delta G^{\ddagger 0}$	ΔV	ΔG^0	$V^{\ddagger}$	$\Delta G^{\ddagger 0}$	ΔV	ΔG^0	$V^{\ddagger}$	$\Delta G^{\ddagger 0}$
HF/6-31G*	−4.71	−5.12	25.41	28.80	−17.94	−18.36	23.87	28.20	−2.53	−3.10	33.46	37.32	−16.67	−2.67	16.13	24.68
MP2(FC)/6-31G*	−23.25	−23.89	6.09	10.03	−32.90	−30.89	4.28	9.71	−2.54	−2.79	9.30	14.97	−19.43	−5.49	5.85	15.01
B3LYP/6-31G*	−19.97	−19.54			−36.39	−34.87			−7.52	−8.46	−1.60	3.41	−25.18	−12.53	−0.32	8.56
CBS-Q	−27.64	−27.87	−2.47	1.05	−40.02	−39.99	−2.76	1.64	−6.49	−6.96	7.27	11.69	−21.96	−7.89	2.95	11.67
G2	−27.28	−27.69	−0.13	3.26	−38.39	−38.53	−0.08	4.25	−6.30	−6.87	8.84	13.32	−21.03	−7.14	5.28	13.77
G3	−26.77	−27.18	−0.04	3.35	−38.78	−38.92	−0.15	4.19	−5.93	−6.51	9.05	13.53	−20.98	−7.10	5.48	13.97
G3S	−28.06	−28.71	−1.69	2.22	−40.65	−39.82	−1.84	3.60								
MMCG3	−28.32	−28.97	−2.06	1.85	−40.99	−40.15	−2.00	3.45								

concentration is 1 mol/L, respectively. We can observe that the four reactions are exoergic and exoergonic in the following order when the multilevel energy methods are used: R2, R1, R4, and R3. It can also be observed in Table 1 that the hydrogen-abstraction classical potential energy barriers are strongly sensitive to the method employed. Although at the HF/6-31G* and MP2(FC)/6-31G* levels all classical potential barrier heights are positive, negative barriers are obtained with the multilevel methods for R1 and R2. This behavior agrees with the fact that in many previous theoretical studies on OH-initiated oxidations of organic compounds negative classical potential energy barriers were also reported.[38−40] It is interesting to point out that at the B3LYP/6-31G* level it was not possible to locate the hydrogen-abstraction saddle points of the two main reactions. Preceding studies have proved the difficulty of correctly describing at the DFT level of theory reactions that occur with a saddle point where the van der Waals forces are important.[41−43] Specifically, these papers show that the search for transition states in radical reactions of abstraction and addition where small size radicals take part (like H or OH radicals) is expensive (in time terms) and problematic. This behavior is found when using different functionals with small basis sets, including in some cases the B3LYP functional.

The results obtained using the multilevel techniques (CBS-Q, G2, and G3) show that the reactions with the lowest classical potential energy barriers are R1 and R2. The difference of energy regarding to the other two possible reactions (R3 and R4) makes these last two processes negligible from a kinetic point of view, in clear agreement with experiments.[2,3] We can also see in Table 1 that the use of multilevel electronic structure methods is necessary to accurately describe these reactions due in part to the fact that a small basis set is used in the geometry optimization. This fact also agrees with previous studies.[44,45] With the purpose of deciding which multilevel method of the first three shown in Table 1 was the most suitable to study the two main hydrogen-abstraction reactions between OH and glycolaldehyde, a calculation of the rate constants using the conventional transition state theory (TST) was carried out as a first test. The results are shown in the three first rows of Table 2 where we can observe that G2 and G3 techniques provide similar results and compare acceptably well to experimental data, whereas CBS-Q values do not compare so well with either of those Gn multilevel techniques or with experimental results. However, the G3 theory represents a new procedure that corrects many of the deficiencies of G2 theory, so this technique should be more suitable for this essay. Anyway, as explained above, the G3S and MMCG3 procedures are more interesting than the original technique from a dynamic point of view. The results obtained with the G3S and MMCG3 techniques are very similar (less than 0.37 kcal/mol of difference in the hydrogen-abstraction classical potential energy barrier heights) leading to the TST

TABLE 2: Rate Constants (in cm^3 molecule^{-1} s^{-1}) at 298 K for Reactions R1 and R2 Using the TST Formulation (Power of 10 in Parentheses)

	k^{TST}	
	R1	R2
CBS-Q	3.48(−09)	1.31(−09)
G2	8.45(−11)	1.59(−11)
G3	7.24(−11)	1.77(−11)
G3S	4.83(−10)	4.69(−11)
MMCG3	9.01(−10)	6.05(−11)

rate constants for reactions R1 and R2 given in the last two rows of Table 2. So then we decided to use the last developed methodology, that is, the G3S technique, for the dynamic calculations presented in this paper.

From here on we will focus our attention on reactions R1 and R2, since we have already checked that reactions R3 and R4 do not have any kinetic relevance. In Figures 1 and 1S (Supporting Information), the MP2(full)/6-31G* and QCISD/6-31G* geometries of the different species involved in reactions R1 and R2 are shown. The geometric parameters obtained with these two methods are very similar, although we find a maximum difference of 0.042 Å in the intermolecular hydrogen bond between OH and glycolaldehyde at the entrance channel complex of R2, and a difference of 7.0 degrees in an intermolecular bond angle between the two products of R1 at the complex on the product side. The hydrogen-abstraction transition-state structures, both for R1 and R2, are more similar to reactants than to products, as it is expected for highly exothermic reactions. The distance between the oxygen of the hydroxyl radical and the abstracted hydrogen in the saddle point of reaction R1 is 1.357 Å at the MP2(full)/6-31G* and 1.368 Å at the QCISD/6-31G* level. For reaction R2, the bond length is 1.327 Å at the MP2(full)/6-31G* and 1.350 Å at the QCISD/6-31G* level. The main component of the eigenvector of the transition state corresponding to the imaginary frequency is due to the approach of the oxygen of the OH radical to the hydrogen that is going to be abstracted, both in reactions R1 and R2. The magnitude of the imaginary frequency is 2077.2i and 1952.3i cm^{-1} for reactions R1 and R2, respectively, at the MP2(full)/6-31G* level, and 1396.7i and 1640.2i cm^{-1} at the QCISD/6-31G* level. This substantial difference between both sets of frequencies is probably due, as mentioned above, to the significant errors involved in the UMP2 vibrational frequencies when even a small amount of spin contamination exists in the UHF wave functions.

In Tables 3 and 4, the energetics of the stationary points of reactions R1 and R2 are shown. From the MEP calculation that was done in both cases at the MP2(full)/6-31G* level, we found a complex in the entrance channel and another complex in the exit channel. Those complexes connect directly with the corresponding saddle points. The complexes toward reactants

TABLE 3: Energies (in kcal/mol) of the Stationary Points for Reaction R1[a]

method	V_{CR}	$(\Delta V_a^G)_{CR}$	$V^{\ddagger}$	$(\Delta V_a^G)^{\ddagger}$	V_{CP}	$(\Delta V_a^G)_{CP}$	ΔV
MP2(full)/6-31G*	−7.03	−5.19	8.01	6.66	−27.66	−26.10	−22.79
QCISD/6-31G*	−6.65	−4.81	5.43	4.10	−22.64	−21.16	−18.38
G3S	−4.71	−2.87	−1.69	−3.04	−31.18	−29.62	−28.06
G3S//QCISD/6-31G*	−4.75	−2.91	−1.54	−2.87	−31.40	−29.92	−28.06

[a] V_{CR} is the classical potential energy of the reactant complex; $(\Delta V_a^G)_{CR}$ is the adiabatic depth of the reactant complex; $V^{\ddagger}$ is the classical potential energy barrier; $(\Delta V_a^G)^{\ddagger}$ is the adiabatic potential energy barrier; V_{CP} is the classical potential energy of the product complex; $(\Delta V_a^G)_{CP}$ is the adiabatic depth of the product complex; ΔV is the classical potential energy of reaction. All energies are relative to reactants.

TABLE 4: Energies (in kcal/mol) of the Stationary Points for the Reaction R2[a]

method	V_{CR}	$(\Delta V_a^G)_{CR}$	$V^{\ddagger}$	$(\Delta V_a^G)^{\ddagger}$	V_{CP}	$(\Delta V_a^G)_{CP}$	ΔV
MP2(full)/6-31G*	−8.62	−6.41	7.16	6.83	−34.48	−31.65	−28.56
QCISD/6-31G*	−7.93	−5.69	5.51	4.29	−35.48	−33.18	−29.97
G3S	−6.09	−3.87	−1.84	−2.17	−44.55	−41.72	−40.65
G3S//QCISD/6-31G*	−6.13	−3.89	−1.72	−2.94	−45.01	−42.71	−41.07

[a] V_{CR} is the classical potential energy of the reactant complex; $(\Delta V_a^G)_{CR}$ is the adiabatic depth of the reactant complex; $V^{\ddagger}$ is the classical potential energy barrier; $(\Delta V_a^G)^{\ddagger}$ is the adiabatic potential energy barrier; V_{CP} is the classical potential energy of the product complex; $(\Delta V_a^G)_{CP}$ is the adiabatic depth of the product complex; ΔV is the classical potential energy of reaction. All energies are relative to reactants.

TABLE 5: G3S Energetics (in kcal/mol) for Reactions R1 and R2[a]

		V ($s=0$)	s (V_{max})	V_{max}	V_a^G (V_{max})	s (V^{AG})	V^{AG}
reaction	R1	−1.69	−0.54	0.81	1.92	−0.69	1.97
reaction	R2	−1.84	−0.37	0.52	2.16	−0.47	2.19

[a] From left to right: classical potential energy at the MP2(Full)/6-31G* saddle point structure; *s* value at the classical potential energy maximum; G3S classical energy barrier height; adiabatic energy at the classical potential energy maximum; *s* value at the adiabatic energy maximum; adiabatic energy barrier height. All energies are relative to reactants. The *s* values are in bohr.

of reactions R1 and R2 are at *s* values of −14.6 and −9.2 bohr, respectively, whereas the complexes toward products are at 9.8 and 18.5 bohr. Both the entrance and the exit complexes are quite far from the saddle point on the MEP, but they involve an important stabilization (see Table 3 and Table 4) with regard to reactants and products due to the hydrogen bond interactions. This stabilization decreases when the ZPE is included. At the G3S and G3S//QCISD/6-31G* levels, the classical potential energy barriers at the LL saddle point structures (MP2/6-31G* and QCISD/6-31G*, respectively) becomes negative. The stabilization of those transition states structures is increased by up to around 1 kcal/mol when ZPE is included.

The results of the G3S single-point energy calculations along the MP2(full)/6-31G* MEP are presented in Table 5. It can be observed that the maximum of the classical potential energy profile has moved to reactants due to the single-point energy calculations made with a HL method along a MEP calculated at a lower level. Moreover, with the G3S technique, we have found a negative classical potential energy barrier at the LL saddle point in both reactions, but the study of the HL potential energy profile shows a positive maximum (V_{max} in Table 5) for R1 as well as for R2. The adiabatic barriers (classical potential energy + ZPE; V^{AG} in Table 5) are still higher and more reactant-like than the corresponding V_{max} values. It is interesting to note that, although V_{max} is higher for the hydrogen-abstraction in R1 than in R2, this order is already reversed when zero-point energy corrections are included (compare V^{AG} values in Table 5).

3.B. Dynamic Results. In this section, the results of the variational transition-state theory rate constant calculation for the hydrogen-abstraction regions of R1 and R2 are presented using several different dual-level methodologies. Next, the association rate constant values for R1 and R2 have been described and the theoretical rate constants for R1 and R2 and the global rate constant and branching ratios of the OH reaction with glycolaldehyde will be compared to the available experimental results.

TABLE 6: Hydrogen-Abstraction Rate Constants (in cm^3 $molecule^{-1}$ s^{-1}, Power of Ten in Parentheses) Calculated with the ISPE Scheme for Reactions R1 and R2

T (K)	k_{H1}	k_{H2}
100	3.80(−16)	5.29(−15)
150	3.47(−15)	8.64(−15)
200	1.33(−14)	1.60(−14)
250	3.35(−14)	2.80(−14)
298	6.43(−14)	4.49(−14)
350	1.11(−13)	6.67(−14)

3.B.1. Hydrogen-Abstraction Rate Constants. 3.B.1.1. ISPE Scheme. As indicated above, the ISPE procedure was used to calculate the rate constants for the hydrogen-abstraction regions of R1 and R2 by using as HL the G3S multilevel method and as LL the reaction path obtained at the MP2(full)/6-31G* level. The canonical variational rate constants with the small curvature tunneling correction ($k_{Hi}(T)(i = 1,2)$) are shown in Table 6. First, the CVT rate constants have been compared with the conventional transition-state rate constants (TST) showing variational effects which follow an opposite trend with temperature in R1 than in R2. For R1, variational effects increase with temperature, whereas for R2, variational effects become less significant at higher temperatures. Tunneling effects are more important for R2 than for R1 because the adiabatic energy profile is wider for R1 (the SCT transmission coefficients are 1.21 and 2.01 for R1 and R2, respectively, at $T = 298$ K). The final hydrogen-abstraction CVT/SCT rate constants turn out to be bigger for R2 than for R1 in the low temperature range (up to around 200 K), but at higher temperatures, the hydrogen-abstraction process which dominates the branching ratio is the one in R1. In comparison with the experimental results for the R1 and R2 rate constants at 298 K, the ISPE scheme is giving too small theoretical rate constants. This underestimation of the rate constant values is mainly due to the fact that when using the ISPE methodology the maximum of the HL adiabatic potential energy profile becomes excessively high. Truhlar and co-workers[27] have attributed this kind of result to a deficiency of the ISPE methodology. If the higher level reaction path differs significantly from the lower level one, then the single-point higher level calculations along the lower level reaction path are not being calculated along the higher level valley floor but rather part way up the valley walls of the higher level valley. These

TABLE 7: Hydrogen-Abstraction Rate Constants (in cm^3 molecule^{-1} s^{-1}, Power of Ten in Parentheses) Calculated with the IOC Scheme for R1 and R2

T (K)	k_{H1}	k_{H2}
100	3.37(−08)	7.52(−08)
150	8.10(−10)	1.42(−09)
200	1.36(−10)	2.05(−10)
250	5.03(−11)	6.73(−11)
298	2.78(−11)	3.42(−11)
350	1.85(−11)	2.11(−11)

ISPE results constitute a first indication that the G3S multilevel method, based on optimized geometries at the MP2(full)/6-31G* level, may not be as appropriate for dynamic calculations using dual-level strategies as it has been shown to be for thermochemical calculations.

3.B.1.2. IOC Scheme. To improve the interpolation algorithm, we have carried out dynamic calculations within the IOC scheme. As indicated above, the interpolations in the IOC procedure are based on information about the reactants, products, and saddle point (or reactant well, product well, and saddle point) at the higher level; the corrected barrier is used at the $s = 0$ position based on a geometry-optimized barrier height obtained from the higher level. Because of computational limitations (the G3S gradients are not available), we have already commented that we cannot carry out a multilevel geometry optimization using the HL (G3S) classical potential energy expression. That is why we are forced to use a kind of intermediate IOC interpolation scheme. In this procedure, the optimization of the stationary point structures and the frequency calculation at these points is performed at the intermediate QCISD/6-31G* level in order to correct the molecular geometry and generalized frequencies along the LL (MP2(full)/6-31G*) reaction path. The HL (G3S) single-point energy calculations are then computed at the QCISD/6-31G* stationary points using this way geometries which should be more similar to the ones obtained at the HL. Another reason to prefer the IOC interpolation rather than the ISPE approach is that the MP2(full) method, used in this case to define the LL MEP, is affected by the spin contamination in open shell systems, providing frequencies higher than expected.[12] In the IOC calculation, this fact may be corrected by using the stationary point frequencies obtained at the QCISD/6-31G* level. The disadvantage of the IOC approach with respect to the ISPE scheme is that the former uses very limited information from the HL PES for the interpolation procedure. The QCISD/6-31G* stationary point geometries have been shown in Figures 1 and 1S (Supporting Information), and we already commented then the small geometric differences observed in comparison to the MP2(full)/6-31G* structures. In Tables 3 and 4, the G3S and the G3S//QCISD/6-31G* classical potential energies and adiabatic energies at the different stationary points for R1 and R2 can be compared. The two approaches give very similar results, with all of the differences being smaller than 1 kcal/mol.

In Table 7, the hydrogen-abstraction CVT rate constants ($k_{Hi}(T)(i = 1,2)$) within the IOC interpolation scheme are presented. Note that, because the hydrogen-abstraction IOC adiabatic barriers for R1 and R2 are −2.14 and −2.25 kcal/mol, respectively, no tunneling effects are present at this level of calculation. The CVT rate constants of the IOC scheme predict large variational effects which decrease the TST rate constants by factors as large as 73.6 at 100 K and by 7.2 at 350 K for R1. The hydrogen-abstraction of R2 turns out to be faster than the hydrogen-abstraction of R1, although k_{H2}/k_{H1} diminishes when temperature increases. This temperature dependence may be explained from an entropic point of view. As it can be observed in Figures 1 and 1S (Supporting Information), the hydrogen-abstraction saddle point of R1 suffers from less steric hindrance than the corresponding saddle point of R2. In this respect, it is interesting to point out that, in R1, the OH radical attacks a hydrogen bonded to an sp^2 carbon, whereas in R2, the hydrogen is bonded to an sp^3 carbon. Moreover, in R2, the OH radical is close to the hydroxyl group of glycolaldehyde which can rotate as temperature increases. These facts make the hydrogen-abstraction saddle point of reaction R2 less favored in entropic terms than the saddle point of R1, especially as temperature increases. The IOC hydrogen-abstraction rate constants ($k_{Hi}(T)(i = 1,2)$) show a negative temperature dependence.

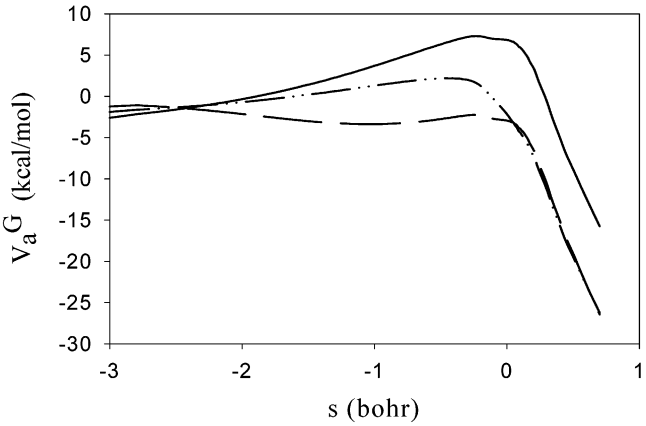

Figure 2. Low-level MP2(full) /6-31G* adiabatic energy curve (—), dual-level ISPE adiabatic energy profile (-••-), and dual-level IOC adiabatic energy profile (− −) along the reaction path for R2. All energies are relative to reactants.

The HL adiabatic potential energy curves at the hydrogen-abstraction regions for R1 and R2 using the IOC interpolation method have a minimum each one which is an artifact caused by the way the IOC interpolation is carried out. In the intermediate IOC interpolation procedure that we have adopted, it is assumed that the width of the classical potential energy profile obtained with the LL (MP2(full)/6-31G*) and the HL (G3S//QCISD/6-31G*) methods is quite similar. However, the shape of the HL and LL adiabatic energy profiles is very different for both R1 and R2 (see Figure 2 in which the ISPE and IOC HL and LL adiabatic energy profiles for R2 as example are shown). The LL adiabatic energies decrease by 12.46 kcal/mol in R1 and by 13.71 kcal/mol in R2 from the V^{AG} location to the reactant complex location on the MEP. In contrast, the HL adiabatic profiles show a decrease of only 0.77 kcal/mol for R1 and 1.64 kcal/mol for R2. These significant differences cannot be completely corrected by an interpolation algorithm based only on information from the stationary points and this is the reason artificial oscillations might appear on the HL interpolated curves using the IOC approach. The classical potential energy corrections at the saddle point structures present values of 9.55 and 8.88 kcal/mol for R1 and R2, respectively, whereas those same classical potential energy corrections at the corresponding reactant complexes are of −2.28 and −2.49 kcal/mol for R1 and R2, respectively. The large classical potential energy correction at the saddle point structures and the change of sign of that correction along the reaction path introduce additional difficulties for the dual-level scheme to handle properly with the high level information only at stationary points. The particular reaction we are studying here, with negative classical potential energy barriers and large variational effects, represents an specially challenging problem for dual-level dynamic methods. It has been recently shown that a quality low

TABLE 8: Rate Constants in cm^3 molecule^{-1} s^{-1} (Power of 10 in Parentheses) and Branching Ratio Corresponding to the R1 Reaction

T (K)	k_{H1}	k_{H2}	k_{AS1}	k_{AS2}	k_1	k_2	k^{CCUS}	branching ratio[a]
100	4.92(−08)	1.08(−07)	9.07(−10)	1.15(−09)	8.91(−10)	1.14(−09)	2.03(−09)	43.9
150	1.04(−09)	1.80(−09)	1.18(−10)	2.01(−10)	1.06(−10)	1.81(−10)	2.87(−10)	37.0
200	1.64(−10)	2.42(−10)	4.94(−11)	9.57(−11)	3.82(−11)	6.87(−11)	1.07(−10)	35.8
250	5.79(−11)	7.67(−11)	3.21(−11)	6.71(−11)	2.12(−11)	3.61(−11)	5.73(−11)	37.0
298	3.12(−11)	3.80(−11)	2.60(−11)	5.70(−11)	1.50(−11)	2.33(−11)	3.83(−11)	39.3
350	2.03(−11)	2.30(−11)	2.33(−11)	5.28(−11)	1.19(−11)	1.66(−11)	2.85(−11)	41.6

[a] See eq 3.

level PES is required to obtain accurate reaction rate constants using the dual-level methodology. We have already mentioned that the MP2(full)/6-31G* level, used as an optimization procedure in the G3S scheme, might not be so appropriate for interpolation purposes at higher levels.

3.B.1.3. Correction to the IOC Scheme. As indicated in the last paragraph, the IOC interpolation that we have been using so far suffers from the problem that the corrected barrier widths are largely determined by the low level calculation. If the topology of the low level PES is qualitatively different from that of the high level, significant errors will occur in the variational and tunneling calculations even though the PES at the stationary points is corrected. The recently developed SIL-1 scheme[34] tries to correct this deficiency. For this reason, in the SIL-1 correction, the range parameter, which determines the width of the corrected classical potential energy profile, is obtained with a calculation at an intermediate level of theory for the classical energy along the reaction path, whereas in the original IOC formulation, that range parameter was determined from the low level MEP. For this purpose, we have used the G3S classical potential energy profile along the LL reaction path, previously employed in the ISPE formulation, and we have obtained a new range parameter for the interpolation functions of the IOC scheme. Note that the original SIL-1 approach was developed for dual-level schemes based on Eckart correction functions. In this work, we have adapted[36] this methodology to the improvement of the cutoff gaussian correction functions which are necessary when the interpolation is carried out from high level calculations at two wells and the saddle point. The new corrected hydrogen-abstraction adiabatic curves show some differences at large s values when compared to the previously obtained IOC interpolated adiabatic profiles but there are not much variation around $s = 0$ where variational effects are expected. The adiabatic barriers in this interpolation scheme are −2.22 and −2.32 kcal/mol for R1 and R2, respectively. The corrected IOC $k_{Hi}(T)(i = 1,2)$ rate constants are given in Table 8 (second and third columns). Their values are somewhat higher than in the original IOC approach but show very similar variational effects and trends with temperature.

3.B.2. Global Reaction Rate Constants. As mentioned above, the DCPs of the association regions for both the R1 and R2 reactions do not present any saddle point. Likewise, no maximum of the adiabatic energy exists neither at the MP2-(full)/6-31G* low level nor at the G3S high level. As a consequence, the entropic contributions are responsible for the appearance of the free energy barriers associated with the canonical variational transition states. The corresponding rate constants k_{AS1} and k_{AS2} are given in the fourth and fifth columns of Table 8. As expected, both k_{AS1} and k_{AS2} slow with the increasing temperature. k_{AS2} turns out to be somewhat greater than k_{AS1}, the ratio between them increasing with the temperature. This behavior is due to the fact that, although both canonical variational transition states at these association regions appear at very long H−O distances, the one corresponding to R1 is somewhat less reactant-like. Then, the enthalpic contribution is more negative for the variational transition state of R1 than for the R2 one, whereas the bottleneck of R1 involves a more negative entropic barrier than the R2 one. So, k_{AS2}/k_{AS1} grows as temperature makes the entropic contribution more and more important.

At this point, the rate constants for reactions R1 and R2 (see the sixth and seven columns in Table 8) can be calculated using eq 2, in which the rate constants k_{CRi} have been variationally evaluated at each free energy minimum of the entrance channel. It can be seen that at low temperatures the association bottleneck is the one that determines the rate constant for each reaction, the abstraction region involving an ostensibly fast rate constant (2 orders of magnitude at 100 K). This is the result of the clearly negative adiabatic barriers corresponding to the abstraction region. However, due to the more negative entropic barriers related with the abstraction bottlenecks (which are quite less reactant-like than the association bottlenecks), the rate constants k_{Hi} become comparable to (and even smaller than) the rate constants k_{ASi} as the temperatures grows. Then both the association and the abstraction regions contribute significantly to the rate constants k_i between 250 and 350 K. On the other hand, the two rate constants k_1 and k_2 have an inverse dependence on the temperature at the whole range of temperatures studied in this work.

Finally, the global reaction rate constant k^{CCUS} for the oxidation of glycolaldehyde by the OH radical and the branching ratio for the reaction R1 have been obtained according to eq 1 and 3, and they are presented in the two last columns of Table 8, respectively. Although the abstraction of the two hydrogen atoms bonded to the non-carbonylic carbon atom (reaction R2) turns out to be the predominant process at whatever temperature, the abstraction of the aldehydic hydrogen atom (reaction R1) also contributes significantly to the global rate constant. The comparison with the experimental studies has to be limited to the results at 298 K, the only experimental available data. Taking into account the huge amount of factors on which the rate constant depends, we have reached a quite good agreement between the experimental value (around 1×10^{-11} cm^3 molecule^{-1} s^{-1}) and the theoretical one (3.83×10^{-11} cm^3 molecule^{-1} s^{-1}). On the other hand, we predict a clear inverse dependence of the global rate constant on the temperature within the range of 100−350 K.

4. Conclusions

In this work, we have combined high level electronic structure calculations with variational transition state theory including multidimensional tunneling corrections when necessary to study the oxidation reaction of glycolaldehyde by the OH radical. In particular, we have obtained the high level classical potential energy by means of the G3S multilevel procedure. In the hydrogen-abstraction regions, we have used stationary point geometries optimized at the QCISD/6-31G* instead of at the MP2(full)/6-31G* level. As for the dynamic calculations, our best results correspond to a kind of intermediate interpolated

optimized corrections (IOC) method as dual level approach for the hydrogen-abstraction regions. In addition, we have adapted the SIL-1 scheme to account for the fact that the width of the classical potential energy profile at the low electronic level differs from the one at the high electronic level, so obtaining corrected IOC rate constants.

In good agreement with the experimental results, we have found that, of the four possible reactions that can occur for the oxidation of glycolaldehyde by OH, only the abstraction of the hydrogen atom bonded to the carbonyl group and the abstraction of the hydrogen atom bonded to the other carbon atom are kinetically significant. Each one of these two reactions begins with an association region without any adiabatic energy maximum that leads to a weak hydrogen bonded complex in the entrance channel. Then an abstraction region with a negative adiabatic barrier follows up to a second complex in the exit channel which is not kinetically relevant due to the high exothermicity of the process. At low temperatures the rate constants of each reaction are essentially determined by the association bottleneck, whereas the entropic effects make both the association and the abstraction bottlenecks contribute significantly to them between 250 and 350 K. The two reactions exhibit an inverse dependence on the temperature at the whole range studied (100−350 K) in this work.

Although Niki et al.[2] have experimentally found at 298 K that approximately 80% of the yield is due to the abstraction of the hydrogen atom bonded to the carbonyl group, our theoretical results predict that the kinetic weight of the abstraction of the hydrogen atoms bonded to the other carbon atom is somewhat more important. Finally, we have to remark that the agreement between the numerical values of our theoretical (3.83×10^{-11} cm^3 $molecule^{-1}$ s^{-1}) and the experimental (around 1×10^{-11} cm^3 $molecule^{-1}$ s^{-1}) at 298 K for the global oxidation reaction of glycolaldehyde by the OH radical turns out to be quite good. This result is highly encouraging if one realizes both the number of factors that have to be accurately introduced in order to calculate the theoretical value and the fact that the experimental results[2,3] were obtained by measuring relative rates with reference to suitable similar reactions.

Acknowledgment. We are grateful for financial support from the Spanish "Ministerio de Ciencia y Tecnología" and the "Fondo Europeo de Desarrollo Regional" through Project Nos. BQU2002-00301 and BQU2001-2935-C02-01. DGEUI of GV projects INF00-15 and INF01-51 is also acknowledged. M.O.-P. acknowledges the Spanish MECD for a FPU grant.

Supporting Information Available: Geometries of the stationary points of reactions R1 and R2 at the MP2(full)/6-31G* and QCISD/6-31G* levels. Energies of the stationary points for reaction R1 and R2 at the G2 and G3 levels. This material is available free of charge via the Internet at http://pubs.acs.org.

References and Notes

(1) Aschmann, S. M.; Arey, J.; Atkinson, R. *J. Phys. Chem. A* **2000**, *104*, 3998.

(2) Niki, H.; Maker, P. D.; Savage, C. M.; Hurley, M. D. *J. Phys. Chem.* **1987**, *91*, 2174.

(3) Bacher, C.; Tyndall, G. S.; Orlando, J. J. *J. Atmos. Chem.* **2001**, *39*, 171.

(4) Truhlar, D. G.; Isaacson, A. D.; Garret, B. C. *Theory of Chemical Reaction Dynamics*; CRC Press: Boca Raton, FL, 1985; Vol. IV, p 65.

(5) Tucker, S. C.; Truhlar, D. G. *New Theoretical Concepts for Understanding Organic Reactions*; Kluwer Academic: Dordrecht, 1989, p 291.

(6) Ochterski, J. W.; Petersson, G. A.; Montgomery, J. A. *J. Chem. Phys.* **1996**, *104*, 2598.

(7) Curtiss, L. A.; Raghavachari, K.; Trucks, G. W.; Pople, J. A. *J. Chem. Phys.* **1991**, *94*, 7221.

(8) Curtiss, L. A.; Raghavachari, K.; Redfern, P. C.; Rassolov, V.; Pople, J. A. *J. Chem. Phys.* **1998**, *109*, 7764.

(9) Curtiss, L. A.; Raghavachari, K.; Redfern, P. C.; Pople, J. A. *J. Chem. Phys.* **2000**, *112*, 1125.

(10) Fast, P. L.; Sánchez, M. L.; Truhlar, D. G. *Chem. Phys. Lett.* **1999**, *306*, 407.

(11) Scott, A. P.; Radom, L. *J. Phys. Chem.* **1996**, *100*, 16502.

(12) Jensen, F. *Chem. Phys. Lett.* **1990**, *169*, 519.

(13) Gonzalez, C.; Schlegel, H. B. *J. Phys. Chem.* **1990**, *94*, 5523.

(14) Garrett, B. C.; Truhlar, D. G. *J. Chem. Phys.* **1979**, *70*, 1593.

(15) Isaacson, A. D.; Truhlar, D. G. *J. Chem. Phys.* **1982**, *76*, 1380.

(16) Frisch, M. J.; Trucks, G. W.; Schlegel, H. B.; Scuseria, G. E.; Robb, M. A.; Cheeseman, J. R.; Zakrzewski, V. G.; Montgomery, J. A., Jr.; Stratmann, R. E.; Burant, J. C.; Dapprich, S.; Millam, J. M.; Daniels, A. D.; Kudin, K. N.; Strain, M. C.; Farkas, O.; Tomasi, J.; Barone, V.; Cossi, M.; Cammi, R.; Mennucci, B.; Pomelli, C.; Adamo, C.; Clifford, S.; Ochterski, J.; Petersson, G. A.; Ayala, P. Y.; Cui, Q.; Morokuma, K.; Malick, D. K.; Rabuck, A. D.; Raghavachari, K.; Foresman, J. B.; Cioslowski, J.; Ortiz, J. V.; Stefanov, B. B.; Liu, G.; Liashenko, A.; Piskorz, P.; Komaromi, I.; Gomperts, R.; Martin, R. L.; Fox, D. J.; Keith, T.; Al-Laham, M. A.; Peng, C. Y.; Nanayakkara, A.; Gonzalez, C.; Challacombe, M.; Gill, P. M. W.; Johnson, B. G.; Chen, W.; Wong, M. W.; Andres, J. L.; Head-Gordon, M.; Replogle, E. S.; Pople, J. A. *Gaussian 98*, revisions A.6 and A.7; Gaussian, Inc.: Pittsburgh, PA, 1998.

(17) Hu, W.-P.; Truhlar, D. G. *J. Am. Chem. Soc.* **1996**, *118*, 860.

(18) (a) Miller, W. H. *J. Chem. Phys.* **1976**, *65*, 2216. (b) Garrett, B. C.; Truhlar, D. G. *J. Chem. Phys.* **1982**, *76*, 1853. (c) Hu, W.-P.; Truhlar, D. G. *J. Am. Chem. Soc.* **1995**, *117*, 10726.

(19) Garrett, B. C.; Truhlar, D. G. *J. Phys. Chem.* **1979**, *83*, 1079.

(20) Garrett, B. C.; Truhlar, D. G.; Grev, R. S.; Magnuson, A. W. *J. Phys. Chem.* **1980**, *84*, 1730.

(21) Garrett, B. C.; Truhlar, D. G. *J. Am. Chem. Soc.* **1979**, *101*, 4534.

(22) Garrett, B. C.; Truhlar, D. G. *J. Am. Chem. Soc.* **1979**, *101*, 5207.

(23) Liu, Y.-P.; Lynch, G. C.; Truong, T. N.; Lu, D.-H.; Truhlar, D. G.; Garrett, B. C. *J. Am. Chem. Soc.* **1993**, *115*, 2408.

(24) Lu, D.-h.; Truong, T. N.; Melissas, V. S.; Lynch, G. C.; Liu, Y.-P.; Garrett, B. C.; Steckler, R.; Isaacson, A. D.; Rai, S. N.; Hancock, G. C.; Lauderdale, J. G.; Joseph, T.; Truhlar, D. G. *Comput. Chem. Commun.* **1992**, *71*, 231.

(25) Pechukas, P. *J. Chem. Phys.* **1976**, *64*, 1516.

(26) Villà, J.; Corchado, J. C.; González-Lafont, A.; Lluch, J. M.; Truhlar, D. G. *J. Phys. Chem. A* **1999**, *103*, 5061.

(27) (a) Duncan, W. T.; Bell, R. L.; Truong, T. N. *J. Comput. Chem.* **1998**, *19*, 1039. (b) Chuang, Y.-Y.; Corchado, J. C.; Truhlar, D. G. *J. Phys. Chem. A* **1999**, *103*, 1140.

(28) Corchado, J. C.; Coitiño, E. L.; Chuang, Y.-Y.; Fast, P.-L.; Truhlar, D. G. *J. Phys. Chem. A* **1998**, *102*, 2424.

(29) González-Lafont, A.; Lluch, J. M.; Bertrán, J.; Steckler, R.; Truhlar, D. G. *J. Phys. Chem. A* **1998**, *102*, 3420.

(30) Villà, J.; Truhlar, D. G. *Theor. Chem. Acc.* **1997**, *97*, 317.

(31) Hu, W.-P.; Liu, Y.-P.; Truhlar, D. G. *J. Chem. Soc., Faraday Trans.* **1994**, *90*, 1715.

(32) Chuang, Y.-Y.; Truhlar, D. G. *J. Phys. Chem. A* **1997**, *101*, 3808.

(33) Chuang, Y.-Y.; Truhlar, D. G. *J. Phys. Chem. A* **1997**, *101*, 8741.

(34) Huang, C.-H.; You, R.-M.; Lian, P.-Y.; Hu, W.-P. *J. Phys. Chem. A* **2000**, *104*, 7200.

(35) Lien, P.-Y.; You, R.-M.; Hu, W.-P. *J. Phys. Chem. A* **2001**, *105*, 2391.

(36) Huang, C.-H.; Tsai, L.-C.; Hu, W.-P. *J. Phys. Chem. A* **2001**, *105*, 9945.

(37) Corchado, J. C.; Chuang, Y.-Y.; Fast, P.-L.; et al. POLYRATE 8.7.2, University of Minnesota: Minneapolis, 2002; http://comp.chem.umn-.edu/WWW/POLYRATE.

(38) Álvarez-Idaboy, J. R.; Mora-Diez, N.; Vivier-Bunge, A. *J. Am. Chem. Soc.* **2000**, *122*, 3715.

(39) Villà, J.; González-Lafont, A.; Lluch, J. M.; Corchado, J. C.; Espinosa-García, J. *J. Chem. Phys.* **1997**, *107*, 7266.

(40) Yamada, T.; Siraj, M.; Taylor, P. H.; Peng, J.; Hu, X.; Marshall, P. *J. Phys. Chem. A* **2001**, *105*, 9436.

(41) Jursic, B. S. *J. Chem. Soc., Perkin Trans. 2* **1997**, 637.

(42) Caballol, R.; Solà, M. *Química Teórica y Computacional*; Andrés, J., Bertrán, J., Eds.; Publicacions de la Universitat Jaume I: Castelló de la Plana, Spain, 2000; p 140.

(43) Bottoni, A.; Della Casa, P.; Poggi, G. *J. Mol. Struct. (THEOCHEM)* **2001**, *542*, 123.

(44) Masgrau, L.; González-Lafont, A.; Lluch, J. M. *J. Chem. Phys.* **2001**, *114*, 2154.

(45) Masgrau, L.; González-Lafont, A.; Lluch, J. M. *J. Chem. Phys.* **2001**, *115*, 4515.